

# LOW-ENERGY ELECTRONIC EXCITATIONS OF THE LAYERED CUPRATES AND THE HUBBARD MODEL

N. BULUT

*Department of Physics, University of California, Santa Barbara,  
CA 93106-9530, USA*

We present a review of the Quantum Monte Carlo results on the magnetic, charge and single-particle excitations as well as the pairing correlations of the two-dimensional Hubbard model. We are particularly interested in how these quantities are related to each other in the metallic state that forms near half-filling. These results are useful in gaining a better understanding of the low energy excitations of the superconducting cuprates.

## 1 Introduction

Superconducting cuprates have many anomalous physical properties [1]. The parent compounds are antiferromagnetic (AF) charge-transfer insulators. Upon finite doping long-range order is destroyed, and a new strongly-correlated metallic state with unusual transport properties forms. In this state there are strong short-range AF correlations. Angular resolved photoemission experiments show that the single-particle properties are heavily damped and strongly renormalized. Charge dynamics probed by various transport measurements are also unusual. Most importantly, a large number of experiments point out that the order parameter of the superconducting state has  $d_{x^2-y^2}$  symmetry [2].

Perhaps, the simplest model that has similar electronic properties is the two-dimensional single-band Hubbard model given by

$$H = -t \sum_{\langle ij \rangle, s} (c_{is}^\dagger c_{js} + c_{js}^\dagger c_{is}) + U \sum_i n_{i\uparrow} n_{i\downarrow}. \quad (1)$$

Here  $c_{is}^\dagger$  creates an electron of spin  $s$  on site  $i$ , in the first term the sum is over near-neighbor sites, and  $n_{is} = c_{is}^\dagger c_{is}$  is the occupation number for electrons with spin  $s$  on site  $i$ . The near-neighbor hopping matrix element is  $t$ , and the onsite Coulomb repulsion is  $U$ .

Here, we will present Quantum Monte Carlo results on the magnetic, charge and single-particle excitations, and the pairing correlations of the Hubbard model in the intermediate coupling regime near half-filling for an  $8 \times 8$  lattice. We will see that a strongly correlated metallic band develops upon doping the antiferromagnetic Mott-Hubbard insulator. This metallic state has anomalous electronic properties. For instance, the quasiparticle properties are strongly renormalized. The system has strong short-range and low-frequency AF fluctuations, and the long wavelength charge response is enhanced. Furthermore, the system exhibits singlet  $d_{x^2-y^2}$  pairing correlations [3,4]. There have been detailed Quantum Monte Carlo and exact diagonalization studies of these properties of the strongly correlated Hubbard or  $t$ - $J$  models. Here, we are especially interested in how these properties are related to each other. We will see that as the AF fluctuations grow, a narrow quasiparticle band, which has a large fermi surface, develops at the top of the lower Hubbard band. The AF fluctuations are also reflected in the effective particle-particle interaction, which is strongly repulsive at large momentum transfers. This feature of the effective interaction along with the large fermi surface causes  $d_{x^2-y^2}$  pairing correlations [3,4,5]. We think that these numerical results are useful in gaining a better understanding of the nature of the low-energy electronic excitations in the superconducting cuprates.

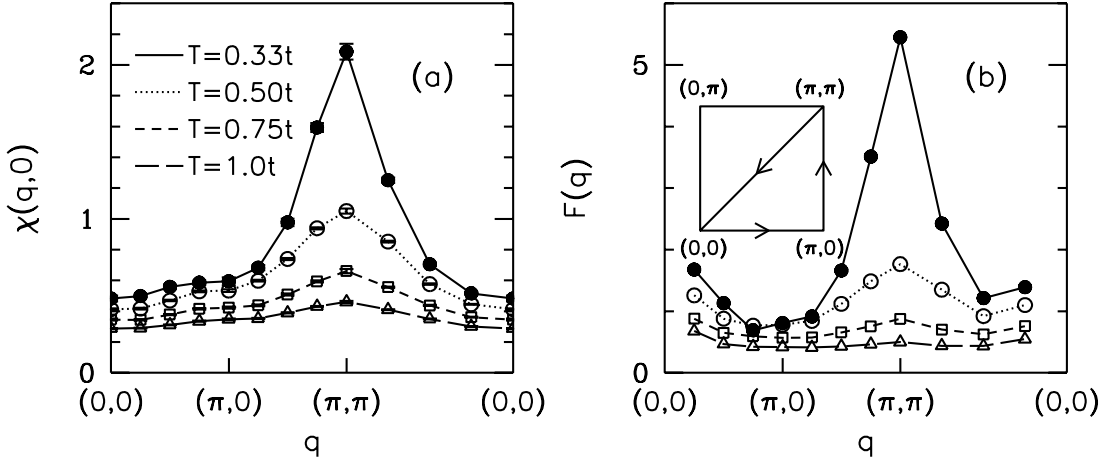


Figure 1: Momentum dependence of (a)  $\chi(\mathbf{q}, i\omega_m = 0)$  and (b)  $F(\mathbf{q})$  for  $U/t = 8$  and  $\langle n \rangle = 0.875$ . Here  $\mathbf{q}$  is plotted along the path show in the inset of (b).

## 2 Magnetic Fluctuations

Using Quantum Monte Carlo simulations [6] we have measured the staggered magnetic susceptibility

$$\chi(\mathbf{q}, i\omega_m) = \frac{1}{N} \sum_{\ell} \int_0^{\beta} d\tau e^{i\omega_m \tau} e^{-i\mathbf{q} \cdot \ell} \langle m_{i+\ell}^-(\tau) m_i^+(0) \rangle. \quad (2)$$

Here  $m_i^+(0) = c_{i\uparrow}^\dagger c_{i\downarrow}$  and  $m_{i+\ell}^-(\tau) = e^{H\tau} m_{i+\ell}^-(0) e^{-H\tau}$ , where  $m_{i+\ell}^-(0)$  is the hermitian conjugate of  $m_{i+\ell}^+(0)$ .

It is useful to have estimates of the characteristic length and energy scales of the AF correlations. For this purpose, in Fig. 1(a) we first show  $\chi(\mathbf{q}, i\omega_m = 0)$  versus  $\mathbf{q}$  for  $\langle n \rangle = 0.875$  and  $U/t = 8$ . We see that as  $T$  is lowered below  $J \simeq 4t^2/U$ , strong AF correlations develop. Next, in Fig. 1(b)

$$F(\mathbf{q}) = \lim_{\omega \rightarrow 0} \frac{\text{Im } \chi(\mathbf{q}, \omega)}{\omega} \quad (3)$$

is shown. Here,  $\text{Im } \chi(\mathbf{q}, \omega)$  has been obtained by numerical analytic continuation [7] of  $\chi(\mathbf{q}, i\omega_m)$ . It is well known that  $F(\mathbf{q})$  is the quantity which determines the NMR  $T_1^{-1}$  response of the system. We see that  $F(\mathbf{q} \sim (\pi, \pi))$  increases rapidly as  $T$  is lowered. The low frequency nature of the AF correlations are also seen in Fig. 2(a), where  $\text{Im } \chi(\mathbf{q} = (\pi, \pi), \omega)$  versus  $\omega$  is plotted. In the cuprates, the longitudinal relaxation rate  $T_1^{-1}$  of the planar Cu nuclei is dominated by the low frequency spin fluctuations near  $\mathbf{q} = (\pi, \pi)$ . On the other hand, because of the form factor of the oxygen hyperfine coupling, the  $T_1^{-1}$  of the oxygen nuclei is mostly determined by the background of  $F(\mathbf{q})$  away from  $(\pi, \pi)$ .

In order to have an estimate of the characteristic length scales, in Fig. 2(b) we have plotted the magnitude of the magnetization correlation function  $|\langle m_z(\mathbf{r}) m_z(0) \rangle|$  as a function of  $\mathbf{r}$  along the  $(1, 0)$  direction. We see that  $|\langle m_z(\mathbf{r}) m_z(0) \rangle|$  decays very rapidly, and the range of the AF correlations are of order a lattice spacing at these temperatures.

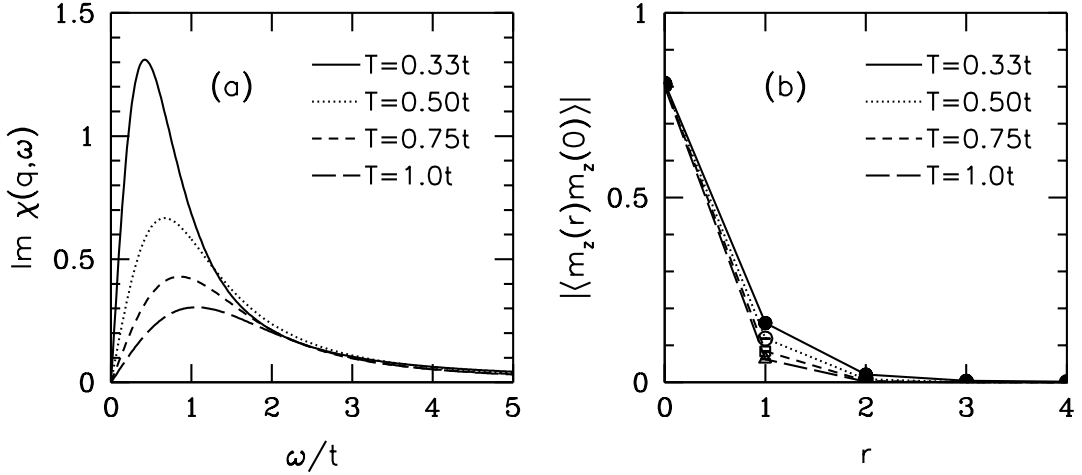


Figure 2: (a) Frequency dependence of  $\text{Im } \chi(\mathbf{q}, \omega)$  at  $\mathbf{q} = (\pi, \pi)$ . (b)  $|\langle m_z(r)m_z(0) \rangle|$  versus  $r$  along the  $(1,0)$  direction. These results are for  $\langle n \rangle = 0.875$  and  $U/t = 8$ .

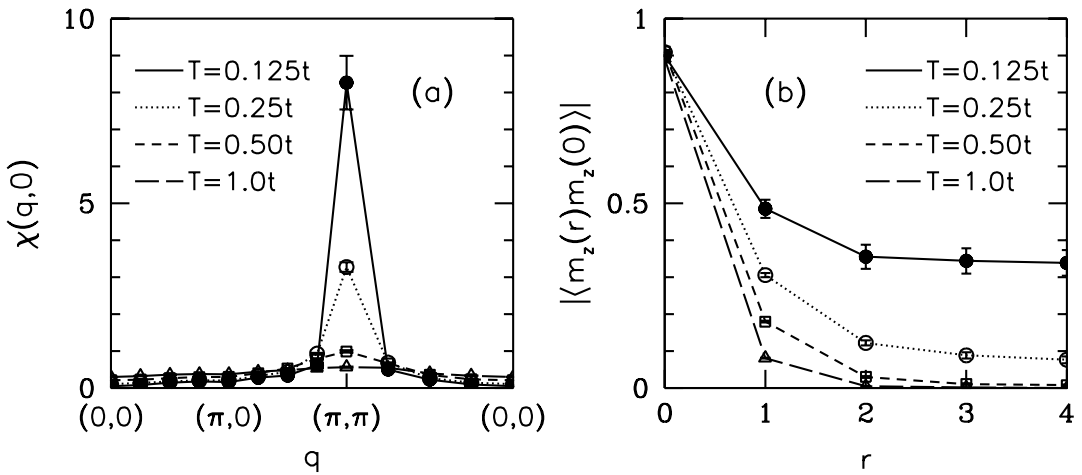


Figure 3: (a) Momentum dependence of  $\chi(\mathbf{q}, 0)$ . (b)  $|\langle m_z(r)m_z(0) \rangle|$  versus  $r$ . These results are for  $\langle n \rangle = 1.0$  and  $U/t = 8$ .

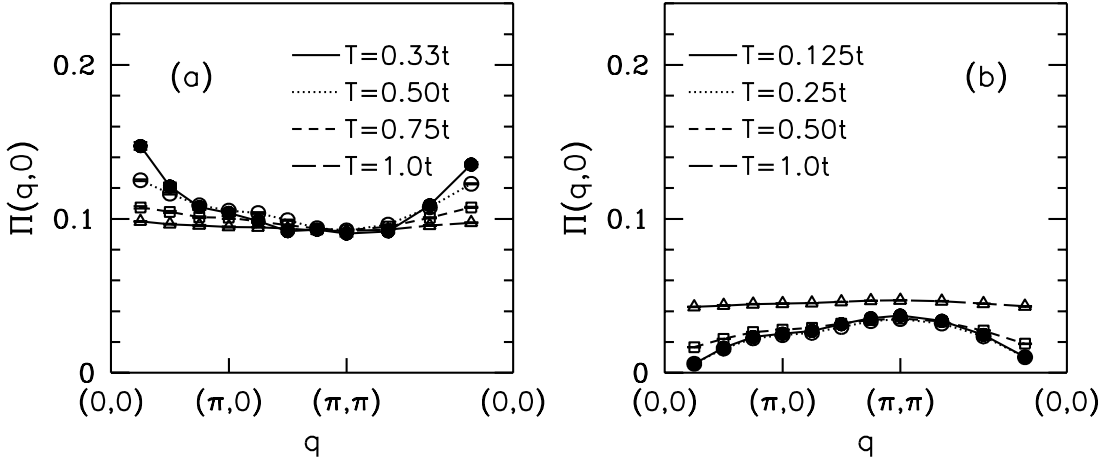


Figure 4: Momentum dependence of  $\Pi(\mathbf{q}, 0)$  for  $U/t = 8$  at (a)  $\langle n \rangle = 0.875$  and (b) 1.0.

These results demonstrate the existence of short-range and low-frequency AF correlations in the metallic state near half-filling. We note that while the AF correlations are short range, there is significant spectral weight under the peak at  $\mathbf{q} = (\pi, \pi)$  as seen in Fig. 1. It is interesting to compare these AF fluctuations with those at half-filling, where the ground state has long-range AF order [8]. Fig. 3 shows results on  $\chi(\mathbf{q}, 0)$  and  $|\langle m_z(\mathbf{r})m_z(0) \rangle|$  at half-filling. At  $T = 0.125t$ , the long-range order is clearly established on the  $8 \times 8$  lattice.

### 3 Charge Fluctuations

In this section, we study the dynamics of the charge fluctuations. We will present results on the charge dynamics obtained from

$$\Pi(\mathbf{q}, i\omega_m) = \int_0^\beta d\tau e^{i\omega_m \tau} \langle n(\mathbf{q}, \tau) n(-\mathbf{q}, 0) \rangle, \quad (4)$$

where  $n(\mathbf{q}, 0) = \frac{1}{\sqrt{N}} \sum_{\mathbf{p}, \sigma} c_{\mathbf{p} + \mathbf{q}\sigma}^\dagger c_{\mathbf{p}\sigma}$ .

Figures 4(a) and (b) show  $\Pi(\mathbf{q}, i\omega_m = 0)$  versus  $\mathbf{q}$  for  $\langle n \rangle = 0.875$  and 1.0. The dependence of  $\Pi(\mathbf{q}, 0)$  on  $U/t$  is shown in Fig. 5(a) for  $\langle n \rangle = 0.875$ . Fig. 5(b) shows the temperature evolution of the charge fluctuation spectral weight  $\text{Im} \Pi(\mathbf{q}, \omega)$  for  $\mathbf{q} = (\pi/4, 0)$  and  $\langle n \rangle = 0.875$ . In these figures, we see that, on the average, the onsite Coulomb repulsion suppresses the charge fluctuations. At half-filling,  $\Pi(\mathbf{q} \rightarrow 0, 0)$  vanishes as the Mott-Hubbard gap opens. However, for  $\langle n \rangle = 0.875$ , the  $\mathbf{q} \rightarrow 0$  part actually gets enhanced, as  $T$  is lowered.

The  $\mathbf{q} \rightarrow 0$  limit of  $\Pi(\mathbf{q}, 0)$  gives the compressibility  $\kappa$  of the system. The low-temperature Monte Carlo studies [9] find that the enhancement of the long wavelength charge response near half-filling is due to the proximity of the system to a metal-insulator transition, and that, as the doping  $\delta$  is reduced,  $\kappa$  diverges as  $\delta^{-1}$ . The enhancement of the long wavelength charge response has many experimental consequences. For instance, the long wavelength phonon modes of a real material can get softened by the enhanced  $\Pi(\mathbf{q}, \omega)$ .

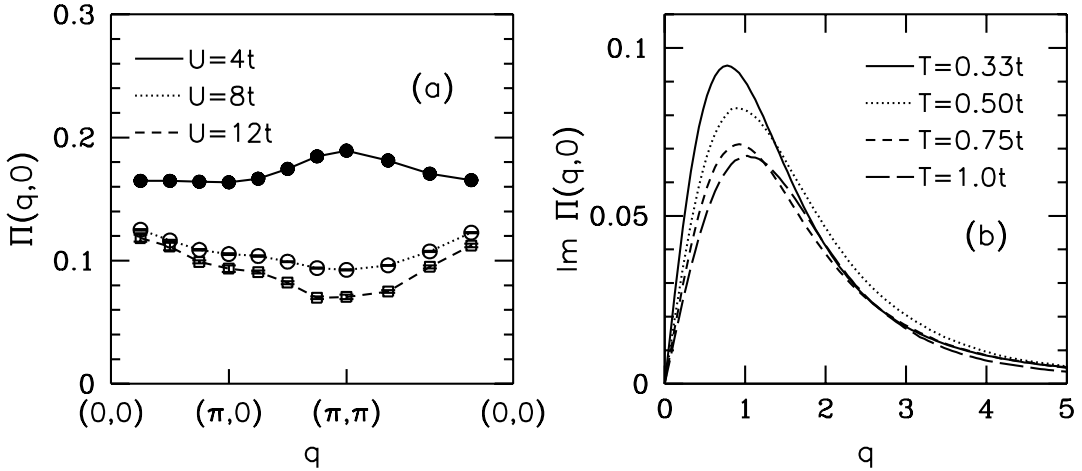


Figure 5: (a)  $\Pi(\mathbf{q}, 0)$  versus  $\mathbf{q}$  for various values of  $U/t$  at  $T/t = 0.5$ . (b)  $\text{Im } \Pi(\mathbf{q}, \omega)$  versus  $\omega$  at  $\mathbf{q} = (\pi/4, 0)$  and various temperatures for  $U/t = 8$ . These results are for  $\langle n \rangle = 0.875$ .

#### 4 Single-Particle Excitations

In this section, we review numerical results on the single-particle excitations [10,11,12]. We are especially interested in the effects of the spin and charge fluctuations on the single-particle excitations. The single-particle spectral weight and the density of states are given by

$$A(\mathbf{p}, \omega) = -\frac{1}{\pi} \text{Im } G(\mathbf{p}, i\omega_n \rightarrow \omega + i\delta) \quad (5)$$

and

$$N(\omega) = \frac{1}{N} \sum_{\mathbf{p}} A(\mathbf{p}, \omega). \quad (6)$$

In order to illustrate how the Coulomb repulsion affects the single-particle properties, in Fig. 6 we show  $A(\mathbf{p} = (\pi, 0), \omega)$  versus  $\omega$  for  $\langle n \rangle = 0.875$ ,  $T = 0.33t$ , and  $U/t = 4$  and  $8$ . Next, the temperature evolution of  $N(\omega)$  is shown in Fig. 7(a). The main features of the spectrum are lower and upper Hubbard bands, and a narrow metallic quasiparticle band at the top of the lower Hubbard band. Surprisingly, the quasiparticle band has strong  $T$  dependence. Comparing this figure with Figures 1 and 4(a), we see that the temperature evolution of the quasiparticle band coincides with the development of the  $\mathbf{q} \sim (\pi, \pi)$  magnetic and  $\mathbf{q} \sim (0, 0)$  charge fluctuations. Fig. 7(b) shows  $N(\omega)$  for  $U/t = 12$  and  $T/t = 0.5$ , where the upper Hubbard band is further split from the lower Hubbard and quasiparticle bands.

Results for  $N(\omega)$  at half-filling are shown in Fig. 8. At  $T = 0.5t$ , we observe a Mott-Hubbard pseudogap in the spectrum. At  $T = 0.125t$ , where long-range order is established on the  $8 \times 8$  lattice, a full single-particle gap is seen. At the moment, it is not completely understood how in the ground state of the system the metallic band, which is seen developing in Fig. 7(a), evolves to the  $N(\omega)$  of the insulating state as the doping is reduced. At the temperatures that the Monte Carlo calculations are carried out, a metallic band forms at the top of the lower Hubbard band even for 3% doping.

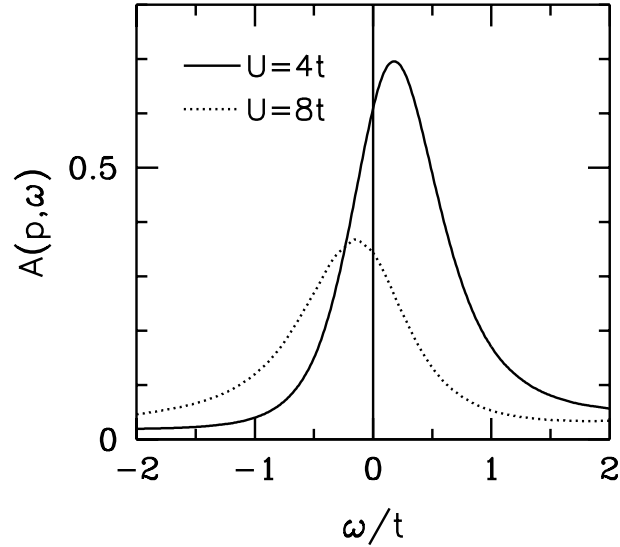


Figure 6: Single-particle spectral weight  $A(\mathbf{p}, \omega)$  versus  $\omega$  for  $U/t = 4$  and  $8$  at  $\langle n \rangle = 0.875$  and  $T = 0.33t$ .

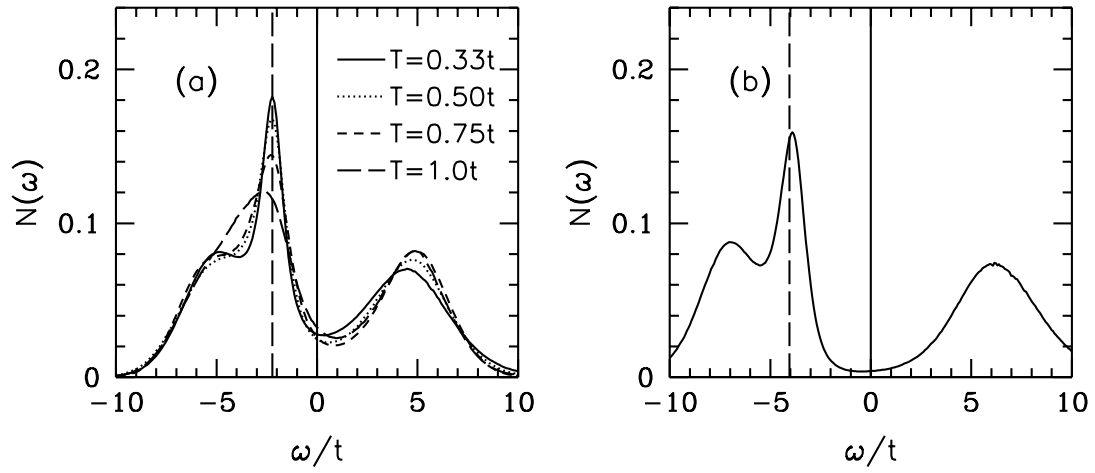


Figure 7: (a) Temperature evolution of  $N(\omega)$  versus  $\omega/t$  for  $U/t = 8$ . (b)  $N(\omega)$  versus  $\omega$  for  $U/t = 12$  and  $T = 0.5t$ . These results are for  $\langle n \rangle = 0.875$ .

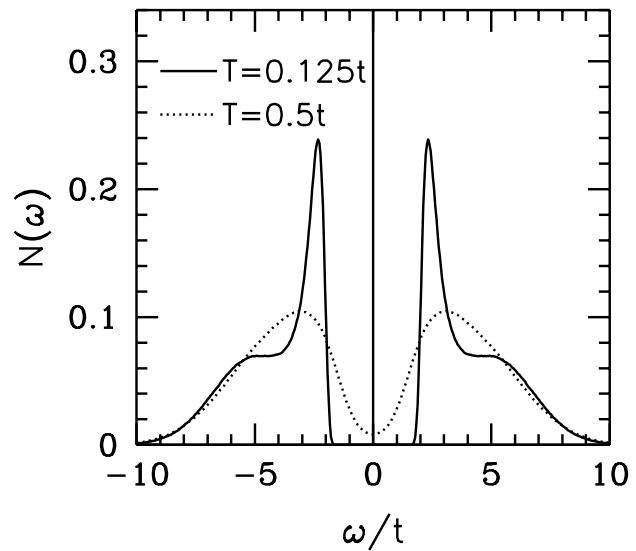


Figure 8:  $N(\omega)$  versus  $\omega$  at half-filling for  $U/t = 8$ .

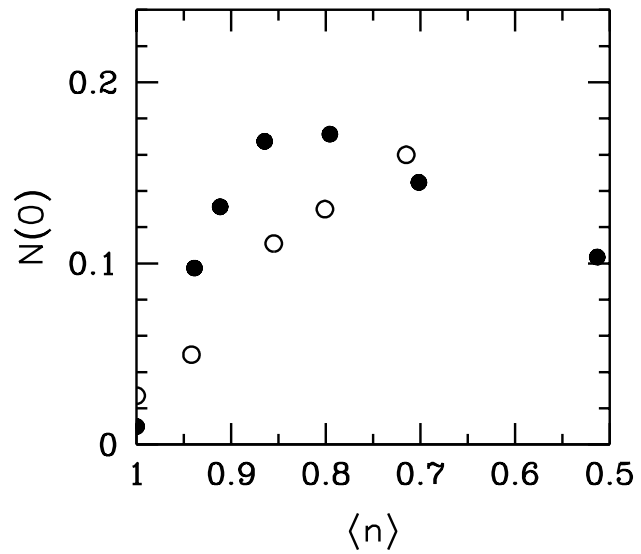


Figure 9: Density of states at the fermi level  $N(0)$  versus the filling  $\langle n \rangle$  for  $U/t = 8$ , and  $T/t = 0.5$  (solid circles) and  $1.0$  (open circles).

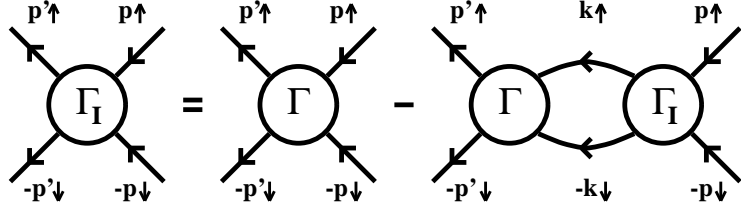


Figure 10:  $t$ –matrix equation relating the reducible and the irreducible interactions in the BCS channel.

Figure 9 shows the filling dependence of the density of states at the fermi level  $N(0)$  for  $U/t = 8$ . At  $T = 0.5t$ , the filling where the maximum of  $N(0)$  occurs is near  $\langle n \rangle = 0.85$ . However, the temperature evolution of the Monte Carlo data indicates that this critical filling will move closer to half-filling as  $T \rightarrow 0$ . In fact, for the simplest Hubbard model that we are using where only the near-neighbor hopping  $t$  and the onsite Coulomb repulsion  $U$  are taken into account, it might occur infinitesimally close to half-filling. Furthermore, simple additional terms in the Hubbard Hamiltonian, such as a next–near–neighbor hopping  $t'$ , might also influence the position of the maximum of  $N(0)$ .

## 5 Pairing Correlations

In this section, we will present results on the effective particle–particle interaction and the solution of the Bethe–Salpeter equation in the BCS channel.

Using Quantum Monte Carlo simulations we have calculated the reducible particle–particle interaction  $\Gamma(p', -p', p, -p)$ , which we will denote by  $\Gamma(p'|p)$  [13]. Here,  $p$  stands for both  $\mathbf{p}$  and  $i\omega_n$ . The reducible interaction is related to the irreducible interaction  $\Gamma_I$  through the  $t$ –matrix equation shown in Fig. 10. In the following, we will present results in the singlet channel where  $\Gamma_S(p'|p) = \frac{1}{2}(\Gamma(p'|p) + \Gamma(-p'|p))$ . Figure 11(a) shows the momentum dependence of  $\Gamma_S(p'|p)$  and  $\Gamma_{IS}(p'|p)$  at  $\omega_n = \omega_{n'} = \pi T$ , corresponding to an energy transfer  $\omega_m = 0$ , for  $U/t = 4$  and  $\langle n \rangle = 0.875$ . In this figure  $\mathbf{p}$  is fixed at  $(\pi, 0)$  and  $\mathbf{q} = \mathbf{p}' - \mathbf{p}$  is swept along the  $(1, 1)$  direction. We observe that both  $\Gamma_S$  and  $\Gamma_{IS}$  peak at large momentum transfers near  $\mathbf{q} = (\pi, \pi)$ . The difference between  $\Gamma_S$  and  $\Gamma_{IS}$  represents the effects of the repeated particle–particle scatterings in the BCS channel. Figure 11(b) shows  $\Gamma_S(\mathbf{q}, 0)$  versus  $\mathbf{q}$  at various temperatures. We see that, as  $T$  is lowered, the  $\mathbf{q} \sim (\pi, \pi)$  part of  $\Gamma_S$  gets enhanced, while the  $\mathbf{q} \sim (0, 0)$  part decreases.

Figure 12 compares the temperature evolution of  $\Gamma_{IS}(\mathbf{q} = \mathbf{p}' - \mathbf{p}, i\omega_m = 0)$  with that of  $\chi(\mathbf{q}, 0)$  for  $U/t = 4$ . We find that  $\Gamma_{IS}(\mathbf{q}, 0)$  shown in Fig. 12(a) can be fit exceptionally well with a phenomenological spin–fluctuation exchange form given by

$$\Gamma_I(q) = U + \frac{3}{2}(gU)^2\chi(q), \quad (7)$$

where the renormalization coefficient  $g \simeq 0.8$ .

$\Gamma_{IS}$  can be used, along with the single-particle Green's function  $G(\mathbf{p}, i\omega_n)$ , to solve the Bethe–Salpeter equation

$$\lambda_\alpha \phi_\alpha(p) = -\frac{T}{N} \sum_{p'} \Gamma_{IS}(p|p') G_\uparrow(p') G_\downarrow(-p') \phi_\alpha(p'). \quad (8)$$

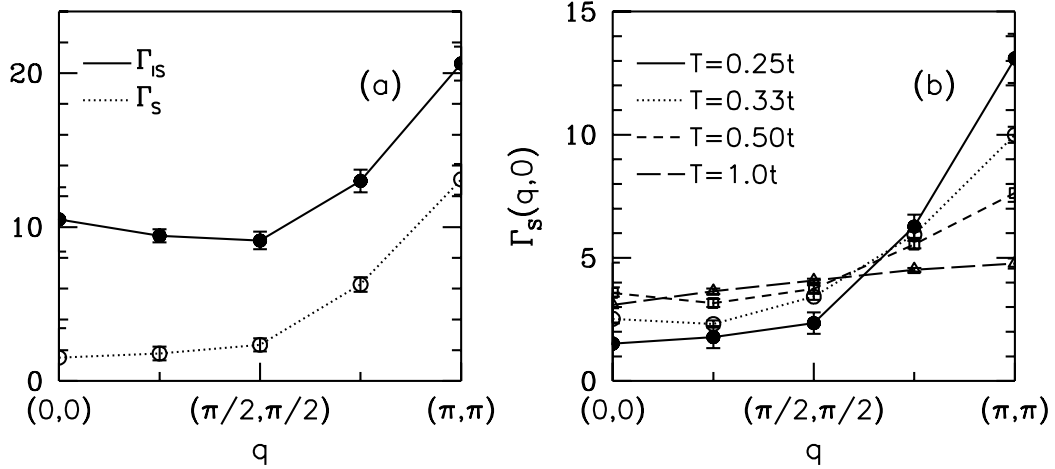


Figure 11: (a) Momentum dependence of the particle-particle reducible and irreducible interactions in the singlet channel,  $\Gamma_s$  and  $\Gamma_{IS}$ , at  $T/t = 0.25$ . (b) Temperature evolution of  $\Gamma_s(\mathbf{q}, 0)$  versus  $\mathbf{q}$ . These results are for  $U/t = 4$  and  $\langle n \rangle = 0.875$ .

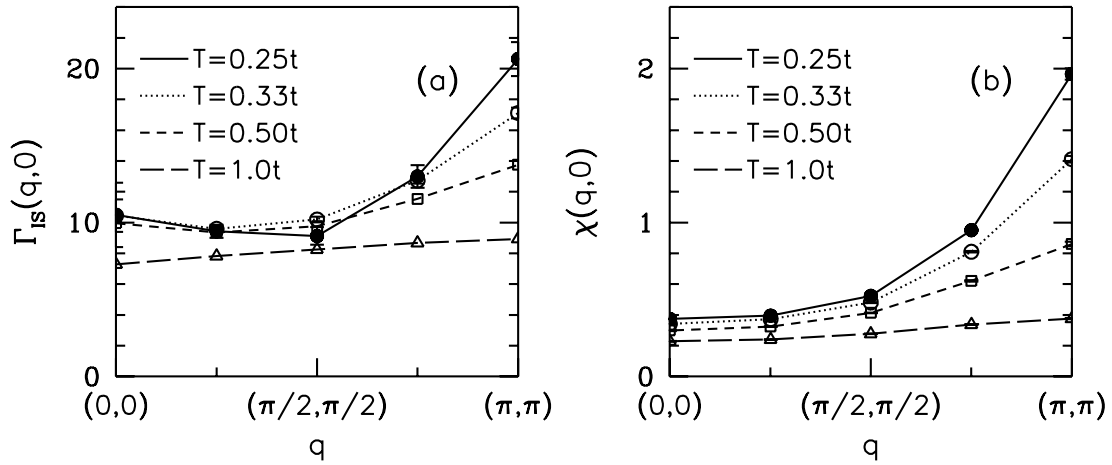


Figure 12: Momentum dependence of (a)  $\Gamma_{IS}(\mathbf{q}, 0)$  and (b)  $\chi(\mathbf{q}, 0)$  at various temperatures for  $U/t = 4$  and  $\langle n \rangle = 0.875$ .

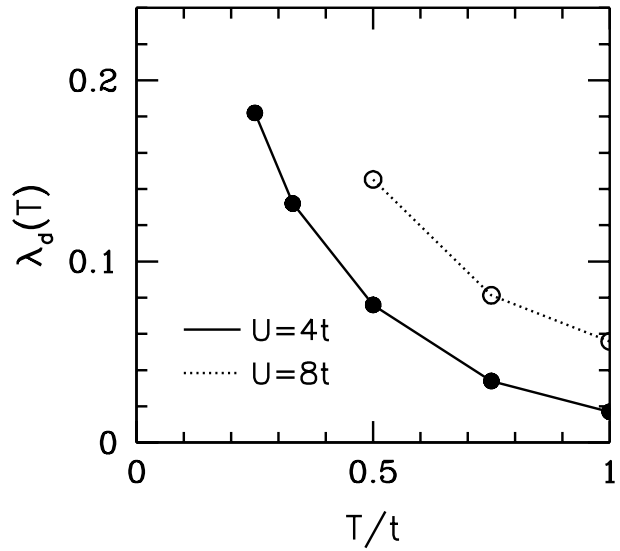


Figure 13: Singlet  $d_{x^2-y^2}$  eigenvalue versus  $T/t$  at  $\langle n \rangle = 0.875$ .

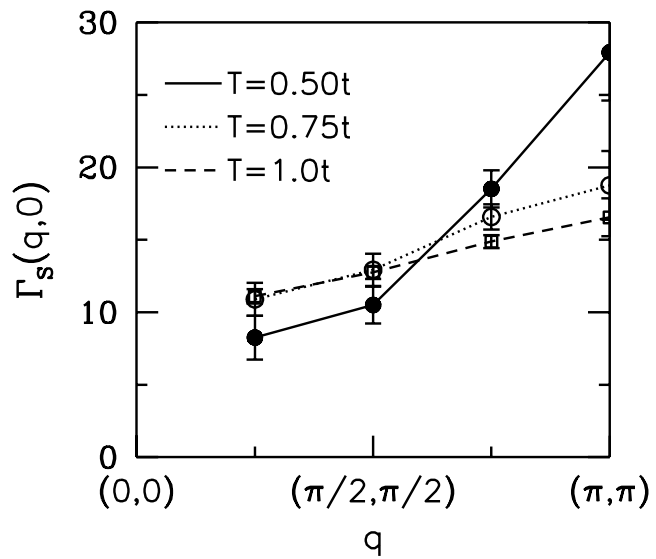


Figure 14: Temperature evolution of the singlet reducible vertex  $\Gamma_s(\mathbf{q}, i\omega_m = 0)$  versus  $\mathbf{q}$  for  $U/t = 8$  and  $\langle n \rangle = 0.875$ .

The irreducible interaction  $\Gamma_{IS}$  is attractive for the solutions which have positive eigenvalues. If the maximum eigenvalue reaches 1, then this signals a particle-particle instability of the system to a superconducting state. At the temperatures that the Monte Carlo calculations are carried out, the eigenvalues are much smaller than 1, and the system is far from a superconducting ground state, if one exists at all. Nevertheless, one can still study which pairing channels are favored as the AF fluctuations develop. We find that, in this regime, the singlet pairing correlations are strongest in the  $d_{x^2-y^2}$  channel. The solid circles in Fig. 13 show the  $d_{x^2-y^2}$  eigenvalue as a function of temperature for  $U/t = 4$  and  $\langle n \rangle = 0.875$ .

For  $U/t = 8$ , we have not been able to calculate the irreducible interaction because of numerical convergence problems, however we have calculated the reducible interaction and the Bethe-Salpeter eigenvalues. Figure 14 shows the temperature evolution of the reducible interaction. Just as for  $U/t = 4$ ,  $\Gamma_S(\mathbf{q}, i\omega_m = 0)$  at large momentum transfers is strongly repulsive, and it grows as  $T$  is lowered. Consequently, the leading singlet pairing correlations occur in the  $d_{x^2-y^2}$  channel. The open circles in Fig. 13 represent the  $d_{x^2-y^2}$  eigenvalue for  $U/t = 8$ .

Finally, we would like to note that the  $d_{x^2-y^2}$  pairing correlations do not necessarily require a long AF correlation length, but simply large weight in  $\Gamma_{IS}$  at momentum transfers near  $\mathbf{q} = (\pi, \pi)$ . For instance, we have seen in Fig. 2(b) that the AF correlation length for  $\langle n \rangle = 0.875$ ,  $U/t = 8$  and  $T/t = 0.33$  is only of order one lattice spacing.

## 6 Conclusions

Numerical studies of the Hubbard model find that a correlated metallic band forms with unusual physical properties upon doping of the insulating half-filled system. Here, we have seen that in this metallic state the single-particle excitations are strongly modified by the many-body effects, the long-wavelength charge response is enhanced, and the system has strong short-range AF fluctuations. Also associated with this state are  $d_{x^2-y^2}$  pairing correlations.

These electronic properties are similar to those of the layered cuprates. Angular resolved photoemission experiments on the cuprates find that the quasiparticles are damped and renormalized. NMR and inelastic neutron scattering experiments show the existence of short-range AF correlations in the superconducting samples. Furthermore, a large number of experiments indicate that the superconducting order parameter has  $d_{x^2-y^2}$  symmetry. For these reasons, we think that simple strongly correlated models such as the two-dimensional Hubbard model are useful in understanding the unusual electronic properties of these materials.

## Acknowledgments

The author would like to thank D.J. Scalapino for many helpful suggestions and discussions. The work presented here was carried out in collaboration with D.J. Scalapino and S.R. White. The author gratefully acknowledges support by the National Science Foundation under grant No. DMR92-25027. The numerical computations reported in this paper were carried out at the San Diego Supercomputer Center.

## References

1. Proceedings of the *10th Anniversary HTS Workshop on Physics, Materials and Applications*, held in Houston, March 12-16, 1996.
2. D.J. Scalapino, *Phys. Reports* **250**, 329 (1995).
3. D.J. Scalapino, E.Y. Loh and J.E. Hirsch, *Phys. Rev. B* **34**, 8190 (1986).
4. N.E. Bickers, D.J. Scalapino, and S.R. White, *Phys. Rev. Lett.* **62**, 961 (1989).

5. D.J. Scalapino, *J. Phys. Chem. Solids* **56**, 1669 (1995).
6. S.R. White, D.J. Scalapino, R.L. Sugar, E.Y. Loh, J.E. Gubernatis, and R.T. Scalettar, *Phys. Rev. B* **40**, 506 (1989).
7. S.R. White, *Phys. Rev. B* **44**, 4670 (1991).
8. J.E. Hirsch and S. Tang, *Phys. Rev. Lett.* **62**, 591 (1989).
9. N. Furukawa and M. Imada, *J. Phys. Soc. Japan* **60**, 3604 (1991); *J. Phys. Soc. Japan* **62**, 2557 (1993); N. Furukawa, F. Assaad, and M. Imada, preprint, cond-mat/9605047.
10. E. Dagotto, A. Moreo, F. Ortolani, J. Riera, and D.J. Scalapino, *Phys. Rev. Lett.* **67**, 1918 (1991); E. Dagotto, F. Ortolani, and D.J. Scalapino, *Phys. Rev. B* **46**, 3183 (1992).
11. N. Bulut, D.J. Scalapino, and S.R. White, *Phys. Rev. Lett.* **72**, 705 (1994); *Phys. Rev. B* **50**, 7215 (1994); *Phys. Rev. Lett.* **73**, 748 (1994).
12. A. Moreo, S. Haas, A.W. Sandvik, and E. Dagotto, *Phys. Rev. B* **51**, 12045 (1995).
13. N. Bulut, D.J. Scalapino, and S.R. White, *Phys. Rev. B* **47**, 6157 (1993); *Phys. Rev. B* **50**, 9623 (1994).